Modeling of ultrasonic wave propagation in composite laminates with realistic discontinuity representation

Andreea-Manuela Zelenyak [a,*], Nora Schorer [a], Markus G.R. Sause [b]

[a] University of Augsburg, Institute of Physics, Universitätsstr. 1 Nord, 86159 Augsburg, Germany
[b] Institute for Materials Resource Management, Mechanical Engineering, Universitätsstr. 1, 86159 Augsburg, Germany

ABSTRACT

This paper presents a method for embedding realistic defect geometries of a fiber reinforced material in a finite element modeling environment in order to simulate active ultrasonic inspection. When ultrasonic inspection is used experimentally to investigate the presence of defects in composite materials, the microscopic defect geometry may cause signal characteristics that are difficult to interpret. Hence, modeling of this interaction is key to improve our understanding and way of interpreting the acquired ultrasonic signals. To model the true interaction of the ultrasonic wave field with such defect structures as pores, cracks or delamination, a realistic three dimensional geometry reconstruction is required. We present a 3D-image based reconstruction process which converts computed tomography data in adequate surface representations ready to be embedded for processing with finite element methods. Subsequent modeling using these geometries uses a multi-scale and multi-physics simulation approach which results in quantitative A-Scan ultrasonic signals which can be directly compared with experimental signals. Therefore, besides the properties of the composite material, a full transducer implementation, piezoelectric conversion and simultaneous modeling of the attached circuit is applied. Comparison between simulated and experimental signals provides very good agreement in electrical voltage amplitude and the signal arrival time and thus validates the proposed modeling approach. Simulating ultrasound wave propagation in a medium with a realistic shape of the geometry clearly shows a difference in how the disturbance of the waves takes place and finally allows more realistic modeling of A-scans.

1. Introduction

New designs of aircrafts, cars or wind turbines are making increased use of composite materials instead of metals [1]. In the metallic parts the occurrence of crack growth within its lifecycle is typically allowed and can be predicted in its consequence using fracture mechanics principles. Composite materials have been investigated for many decades, but because their structure combines the properties of more than one constituent material, the damage evolution and their failure mode is not as well understood as it is in the case of metallic structures [2,3]. Due to these difficulties, in fiber reinforced composites the occurrence of inter-ply delamination is only tolerated up to a certain geometrical dimension [2]. Modern fiber reinforced composite materials can have different textile architectures, including stacking of unidirectional fiber plies at different angles, woven fabrics or 3D-textiles such as stitching, crocheting and many more. Furthermore, each ply can be made from different fibers and may contain additional impurities such as fabrication residues or binder materials. In addition, the final composite structure may also include different types of defects like pores, inter-fiber cracks, inter-ply or intra-ply delamination, fiber breakage, ondulations and many more [3]. Delamination can occur due to multiple reasons, ranging from malfunctions in the production process to in-service damage such as impact. As it is compromising the local structural integrity of the composite laminate and may grow substantially at low level fatigue load [4,5], the detection of delamination is one of the most relevant tasks to non-destructive testing (NDT) approaches.

The most commonly used NDT techniques for the defect detection in composite materials are: active ultrasonics, lock-in thermography, shearography, guided wave testing and radiography [6–11]. Active ultrasonic testing (UT) is a well-known and established technique but the detection sensitivity relative to the delamination shape, orientation, general material microstructure is still under investigation [12]. Probability of detection (PoD) is

* Corresponding author.
  E-mail addresses: andreea-manuela.zelenyak@physik.uni-augsburg.de (A.-M. Zelenyak), nora.schorer@physik.uni-augsburg.de (N. Schorer), markus.sause@mrm.uni-augsburg.de (M.G.R. Sause).

usually used as a metric to quantify the reliability of the UT method [13–17]. Estimation studies for PoD curves rely mostly on many experimental trials of the UT procedure using reference specimens with artificial defects. Given the statistical approach used this can be fairly time consuming and, including the costs for the specimen fabrication, also quite expensive. More recently it was proposed to perform such estimations of PoD curves using modeling assistance, hence called MaPoD [18–23]. In order to optimize the UT equipment parameters and to decrease the costs for experimental work much recent research is focused on developing predictive and quantitative numerical models for UT [24–36].

Usually when numerical models are implemented to simulate ultrasonic wave propagation in a composite material, the material microstructure and defect representation suffers a lot from geometric simplifications. This is due to the complexity of the topology, which is fairly inconvenient to reproduce by using only Computer Aided Design (CAD) tools. The topology of internal defects is simplified in most modeling approaches as being round, elliptical, or perfectly flat [37–39]. In experimental UT signals multiple echoes are present due to the complex topology of the defects, such as reflections given by the corners or by two contiguous faces [40]. This kind of detail can easily be present when testing delamination and may have an impact upon the interpretation of the inspection result.

Internal geometry reconstruction of defects from magnetic resonance imaging (MRI) or from computed tomography (CT) can be done using various commercial software packages such as "Simpleware Ltd." or "Materialise Mimics". This results in sophisticated discretized approximations of the volumetric topology of the scanned defect. Surface or volume meshes can be generated from such three-dimensional imaging and can then be used as geometry in numerical modeling tools [41,42].

The present investigation aims to solve the question, whether the particular topology of inter-ply type delamination needs to be accounted for in quantitative numerical modeling of UT. Therefore, a validation scheme to properly implement the UT method in numerical methods is briefly described. Subsequently, an example is presented to perform a geometry reconstruction for a delamination type defect. This makes use of the "Volume Graphics (VG studio Max)" software for visualization and extraction of the computed tomography data. The obtained surface mesh is then post-processed using "MeshLab". Finally, the geometry is implemented in a validated finite element method (FEM) approach using the "Comsol Multiphysics" platform. This approach is meant to demonstrate how the real geometry of an embedded defect interacts with the numerical simulated ultrasonic field. Experiments are then used to validate the accuracy of the numerical model by direct comparison of the modeled and the experimental A-scan signals.

2. Experimental

The plate specimen is fabricated as unidirectional prepreg laminate with a layup configuration of eight plies $[0]_{4sym}$ using the carbon/epoxy system Sigrafil CE1250-230-39. Multiple artificial delamination areas are created by including bags made from 25 μm thick Ethylene tetrafluoroethylene (ETFE) foil at different locations. These are embedded in the laminate prior to curing at the designated locations. X-ray computed tomography and ultrasonic testing is carried out to validate the positions of the artificial delamination. The CT scans were performed using a CT scanner (Nanotom 180, GE systems) with a tube voltage of 80 kV and a tube current of 160 μA. The data was reconstructed using the "Phoenix datos|x2" software. An exemplary CT scan of the probe is shown in Fig. 1 where the delamination can be seen being present at 0.56 mm in the laminate sample between ply No. 3 and 4 from the top surface.

The UT inspection measurements were conducted using an ultrasonic system (USM go+, GE systems) and the single element transducer (V 201-RM, Olympus) operating in pulse-echo mode. For the inspection of the 1.87 mm thick laminate, a delay line made of polystyrene (DLH-1, Olympus) was used to allow far-field inspection conditions. A viscous couplant (Couplant B-Glycerin, Olympus) was used between the delay line and the transducer as well as in contact to the composite specimen to increase the transmission of the ultrasonic waves. A square-wave pulse with 100 ns width was used to generate the ultrasonic waves at a center frequency of 5 MHz. The initial pulse was triggered with 500 Hz repetition frequency. All signals were received with a gain of 34.2 dB. The calibration of the experimental setup was done using a steel step wedge according to ASTM E797.

The experimentally investigated areas are those in the area of the artificial delamination, but also reference areas, where no artificial defects were present. The latter is used for validation of the composite material model. Measurements were carried out at different locations in the region of the artificial delamination (cf. Fig. 2a), as additional challenges of the ultrasonic measurements arise due to edge effects [43]. For each location a total number of five A-Scan signals were recorded.

Examples of the A-scans are shown in Fig. 3. In Fig. 3a the reference signal in a region without artificial delamination is plotted. Besides the surface echo (SE) the signal predominantlly yields the 1st and 2nd backwall echo (BWE) given by the first and second reflection at the specimen bottom. In Fig. 3b the A-scan is taken at the location when the transducers is at position offset to the right of the delamination area (III). The signal shows the presence of the SE, BWE but also an echo given by the presence of the delamination (DE), which is located between SE and BWE in the immediate vicinity of the SE. Based on the longitudinal sound velocity of 3133 m/s in the out-of-plane direction of the composite this yields a depth location of 0.64 mm, which is in good agreement with actual position of 0.59 mm as obtained from the CT measurements.

3. Numerical modeling of ultrasonic testing

Modeling ultrasonic testing of a composite material sample includes three important steps: transducer modeling, wave propagation modeling and realistic description of the internal discontinuities. All steps need to be validated through experimental results. The entire modeling concept followed herein is summarized in the scheme presented in Fig. 4.

Because of the electromechanical coupling between ultrasonic waves in solids and fluids and the piezoelectric effect for converting the detected wave into an electrical signal, multiphysics approaches are needed to perform quantitative modeling of ultrasonic testing. Commercial multiphysics FEM platforms are already being used with great success to model ultrasonic wave propagation and its interaction with the complex material structure [44–49].

3.1. Transducer implementation

3.1.1. Geometry implementation

In order to obtain realistic results from the FEM approach, the model setup should reflect as much as possible the experimental conditions. For this reason, a realistic transducer model is introduced in the FEM environment. In accordance with our experimental setup, a V201 RM type transducer from Olympus was modeled. It represents a typical single element contact transducer with an attached delay line. The level of detail to reconstruct the trans-
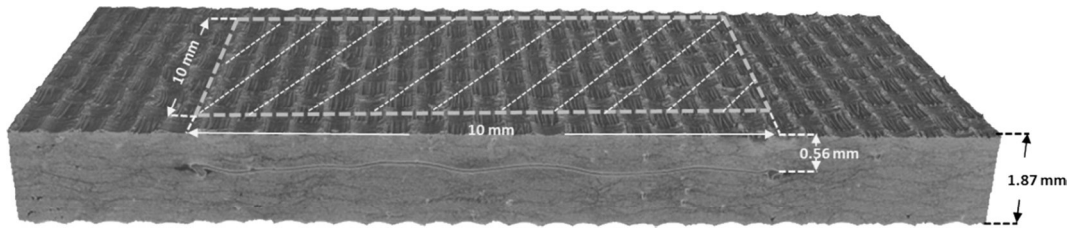
Fig. 1. 3D-representation of the test specimen with embedded artificial delamination and dimensional details.
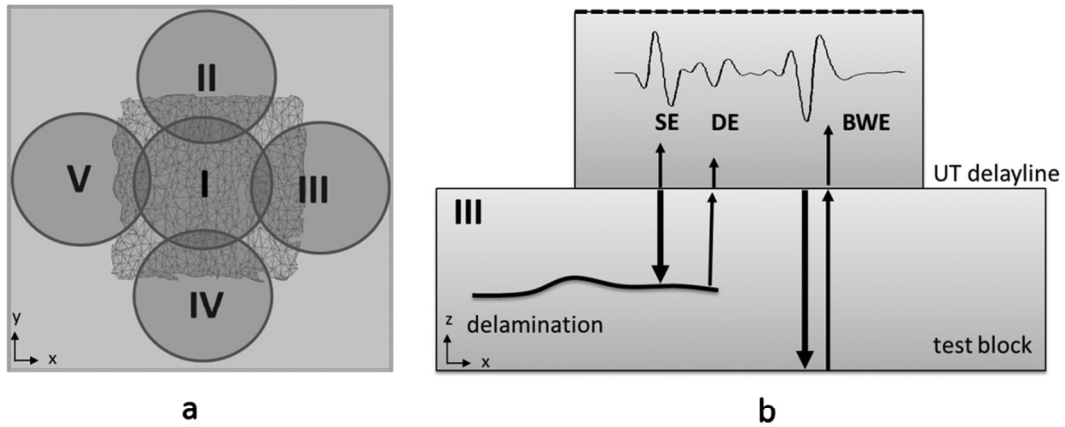

Fig. 2. Scheme of the transducer positions above the artificial delamination during experiments (a) and partial reflection at delamination edges (b).
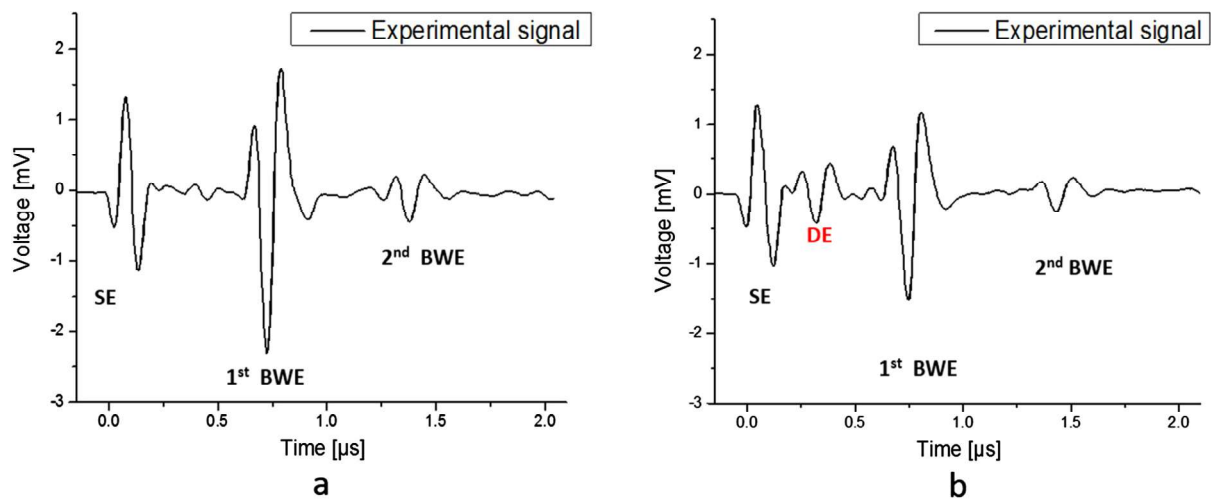

Fig. 3. Typical experimental A-scan signals for the composite laminate (a) versus transducer position III, partially above artificial delamination (b).
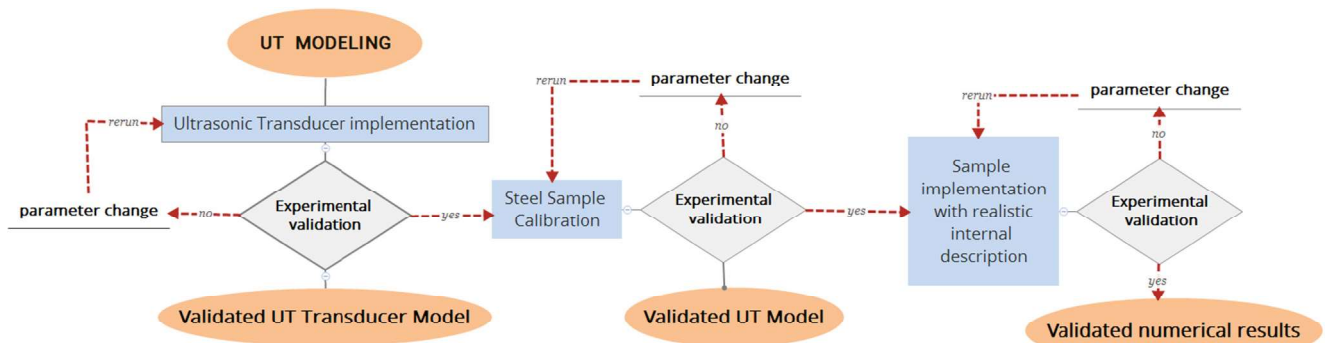

Fig. 4. Proposed model validation concept for ultrasonic testing.

ducer requires a very high precision for the dimension extraction. In parametric studies it has been noticed that just a few μm deviations of geometric details can induce substantial differences in the A-scan amplitude or can shift the arrival time.

We decided to extract the transducer dimensions from CT scans, component identification being made based on the material densities. All modeling relevant parts are presented in a cross-sectional view with different colors in Fig. 5a. All extracted dimensions were subject to parametric analysis, taking into the account the CT measurement accuracy. Reference of this parametric study was made against a measurement carried out on a steel plate (see Section 3.1.2). Finally, some geometric details and components were found not to induce significant change of the A-scan and were hence not modeled (e.g. sensor casing) or were reduced in size (e.g. backing mass) to increase the computational efficiency of the model. In addition, a 2D axial symmetric representation is chosen (see Section 3.2.2 for coupling to 3D model). The final dimensions used are those seen in Fig. 5b.

3.1.2. Material properties, applied physics and discretization settings

The material properties used for the transducer components were extracted from datasheets, literature and the material library in "Comsol Multiphysics". The most important properties were those of the piezoelectric element and those of the backing mass. For the piezoelectric material, PZT 5A with the specific values imported from the material library was chosen (cf. Table 1). The backing mass uses also the material properties of the PZT 5A given in Table 1 with the electric coupling matrix manually defied as having all components equal to 0 C/m² . The mechanical damping of the backing mass was defined using Rayleigh damping parameters $\alpha = 2 \times 10 + 6 \, s^{-1}$ and $\beta = 1 \times 10^{-9}$ s as result from a parametric optimization study. The delay line was defined as being made from polystyrene (cf. Table 1).

An electrical excitation is defined through a piecewise function, V(t), and applied as voltage source to the top surface of the active piezoelectric element using the "AC/DC module" of "Comsol Multiphysics". The pricewise function V(t) is using a sub-function which represents a Gaussian pulse with 100 ns width applied to the specified time interval as can be seen in Eq. (1).

$$V(t) = \begin{cases} -8 \cdot 10^7 \exp^{-(t-3\cdot10^{-8})^2/1\cdot10^{-16}} & t \in [0\ldots1.5\cdot10^{-8}] \\ -8 \cdot 10^7 \exp^{-(t-1.5\cdot10^{-8})^2/2.5\cdot10^{-15}} & t \in [1.5\cdot10^{-8}\ldots2\cdot10^{-7}] \\ 0 & t \in [2\cdot10^{-7}\ldots10\cdot10^{-6}] \end{cases}$$

(1)

Table 1
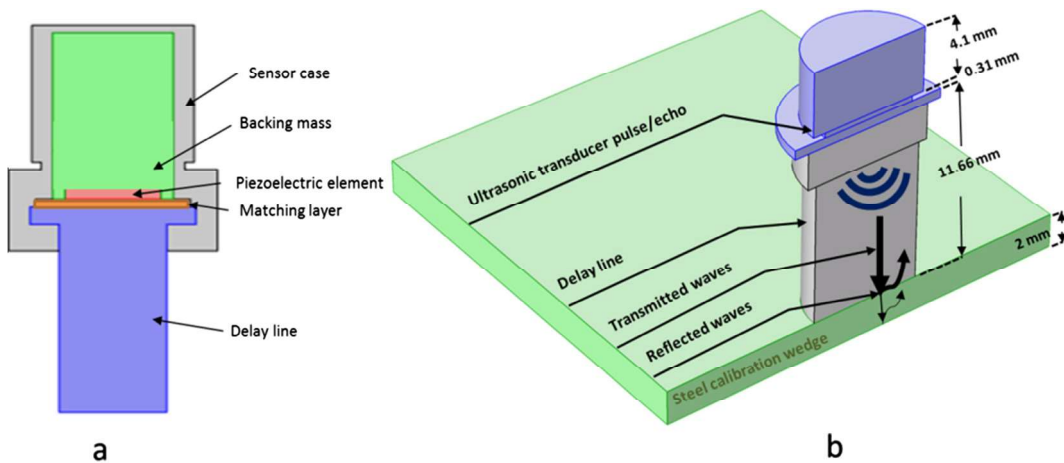Elastic and piezoelectric properties of the materials used in transducer simulation. Subscript indices follow the conventions of piezoelectric materials.

Property	PZT-5A	Polystyrene
Density, ρ [kg/m³]	7750	1050
Elastic modulus [GPa]	$C_{11} = C_{22} = 120.3$	3.77
	$C_{13} = C_{23} = 75.1$	
	$C_{33} = 110.9$	
	$C_{44} = C_{55} = 21.1$	
	$C_{66} = 22.6$	
Poisson ratio	–	0.34
Piezoelectric constants, S_{ikm} [C/m²]	$S_{31} = S_{32} = -5.4 \; S_{33} = 15.8$	–
	$S_{24} = S_{15} = 12.3$	
Electrical permittivity, χ_{im}	$\chi_{11} = 919.1$	–
	$\chi_{22} = 919.1$	
	$\chi_{33} = 826.6$	

An electrical ground is chosen on the opposite side. A half-bridge P-SPICE circuit model (cf. Fig. 6) is attached via a terminal boundary constraint to consider the electrical impedance load of the attached electronics. Initially, the voltage is applied across resistor R1, resulting in an emission of a 5 MHz pulse. The values for the input impedance found in Fig. 6a were established running parametric studies. Detection of the A-scan signals is made as voltage measurement across resistor R2. By solving the coupled piezoelectric equations, the applied electrical boundary conditions result in an ultrasonic wave, which propagates along the delay line and finally into the sample. The ultrasonic wave propagation is solved using the solid representation in the "structural mechanics module" in "Comsol Multiphysics", which takes into account all reflections given by acoustic impedance changes and discontinuities such as the boundaries or voids.

For modeling acoustic wave propagation at 5 MHz frequency, all sensor parts require a very high mesh resolution. The dimensions of the individual elements should be only a fraction of the wavelength [38], otherwise numerical dispersion effects are expected to arise and to induce mismatches against the experimental signal [50]. Convergence studies were carried out for all sensor parts to establish the sufficiency of the mesh size and the time step following the self-referencing approach established in [49]. In the end, for each material the maximum element size was defined to be $\leq\lambda/5$ with λ being the shortest relevant wavelength. As time step, 2 ns was found to provide a convergent solution.

To finally validate the transducer implementation, an ASTM E797 steel block was used. Parametric studies were carried out
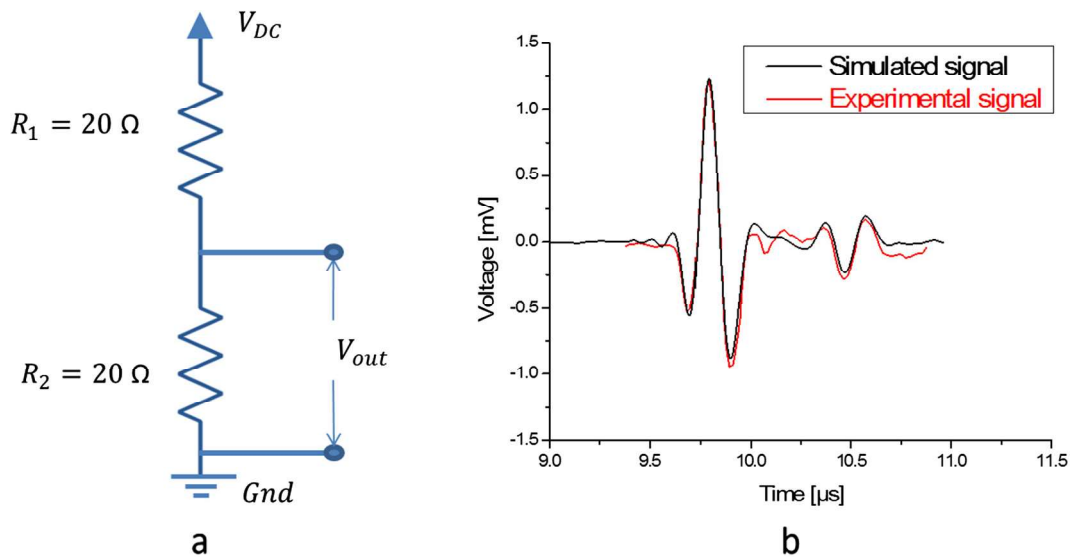

Fig. 5. Transducer model in cross-sectional view (a) and model validation using A-scan on steel plate (b).

Fig. 6. Half-bridge P-Spice circuit model (a) and comparison of A-scan measured on steel plate to modeling result (b).

for geometric details, material properties and discretization settings referencing against the experimentally recorded A-scan. The finally achieved quantitative agreement in the voltage scale of both A-scan signals can be seen in Fig. 6b.

3.2. Composite sample

3.2.1. Geometry implementation

A first decision needs to be made to account for the specific fiber arrangement in the material. For continuous fiber reinforcement, this generally consists of suitable representation of the stacking orientations, the textile microstructure and homogenization thereof. For short and long fiber reinforcement the material model needs to be homogenized using 1st or 2nd order approximations considering the specific orientation tensor of the fibers [51,52]. For the present case this is not further emphasized, as the unidirectional stacking facilitates the use of a homogenous continuum model. An additional challenge arises from the geometrical representation of internal discontinuities. This can be done via artificial geometric representation (spheres, ellipsoids, planes, etc.) or in a direct approach using volumetric imaging of the real geometry. The work-flow for implementing a discontinuity that way is presented schematically in Fig. 7. In our case, the extraction routine uses two software packages to yield a discretized geometric representation suitable for numerical computations in "Comsol Multiphysics".

The first step in converting volumetric images into a geometry suitable for FEM computation is a segmentation routine. This was done within the software "VG Studio Max 2.1". For segmenting internal discontinuities, threshold based methods are typically applied to classify the scan into regions of interest based on their gray scale values, contrast level, brightness or even texture [53]. This step is fairly critical in preserving the overall geometry of the region of interest. Severe over- or underestimation can happen when inappropriate threshold values are used. Hence, a broad range of concepts, such as active contours, snakes contours, wave propagation or active shape models have been proposed to solve this problem [54–62]. The work within "VG Studio Max 2.1" is done in four main steps. The gray-value based image segmentation is the first step and is used to divide the volume data into the "Regions of Interest" (ROIs). This can be done automatically by entering the gray isosurface value or manually by selecting repre-

sentative sections of material and background. For the typical kind of discontinuity this is fairly convenient, as cracks and voids basically have the density values of air. Once the discontinuity is segmented from the rest of the structure the ROI extraction is done. Using the "Surface Extraction" tool a surface mesh is generated from the volume data set and exported as "Stereolithographic File" (STL) which represents a surface mesh formed of triangles. For this geometry extraction process a "Normal" quality of the mesh network in "Quick mesh" generation mode proved sufficient to preserve the geometrical dimensions of the artificial delamination discussed exemplarily in the following. In Fig. 8 the extracted delamination in STL format is presented. Theoretically, this surface mesh could be directly imported into a FEM program as geometric object. However, the volumetric data suffers from imperfections during the detection stage (artefacts, resolution, etc.), which affects the quality of the extracted surface mesh. A lot of defects can be present in the exported mesh structure, such as small holes, inclusions, deformed mesh elements, self-intersecting surfaces and isolated entities. The necessity of an additional step for editing, cleaning, inspecting, and "healing" this kind of mesh defects is somehow obvious considering the example in Fig. 8. A suitable tool to this end was found to be "Meshlab" which is an open source software dedicated to process and edit unstructured 3D triangular meshes.

In order to have a continuous and topologically well-defined mesh geometry for the FEM environment the CT extracted mesh needs to be processed in several ways. In the following, we present and discuss the typical steps done within the "MeshLab" environment for the example of Fig. 8.

3.2.1.1. Cleaning and repairing. Different aspects may render the surface mesh useless for numerical computations. For an internal discontinuity the surface is required to be continuous. However, when a part of the surface mesh collides with another part of itself it destroys the integrity of the mesh generating so-called *self-intersection faces.* Another critical situation for the mesh continuity is any edge connected to more than two faces that is the mesh becomes *non manifold* (see Fig. 7). Within "MeshLab" filters are included which allow to automatically select and remove such parts of the mesh. A related step is the removal of isolated mesh pieces whose diameter is smaller than a specified value. This effectively eliminates small mesh parts which do not significantly con-
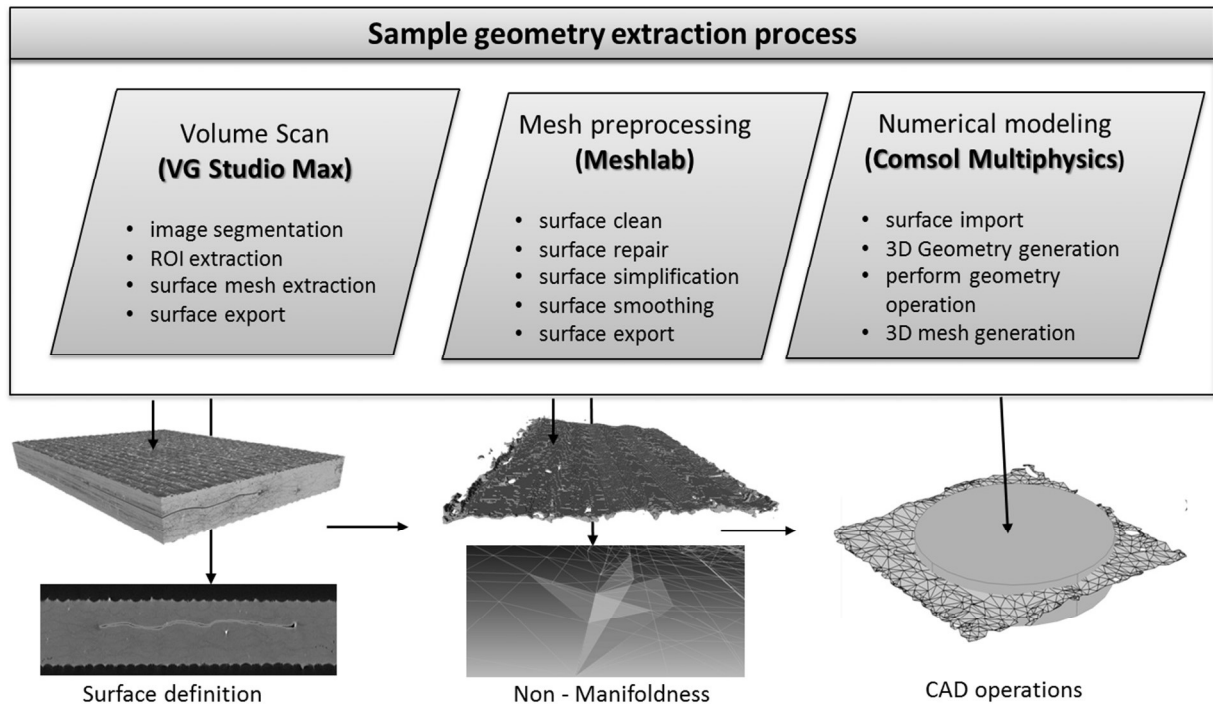
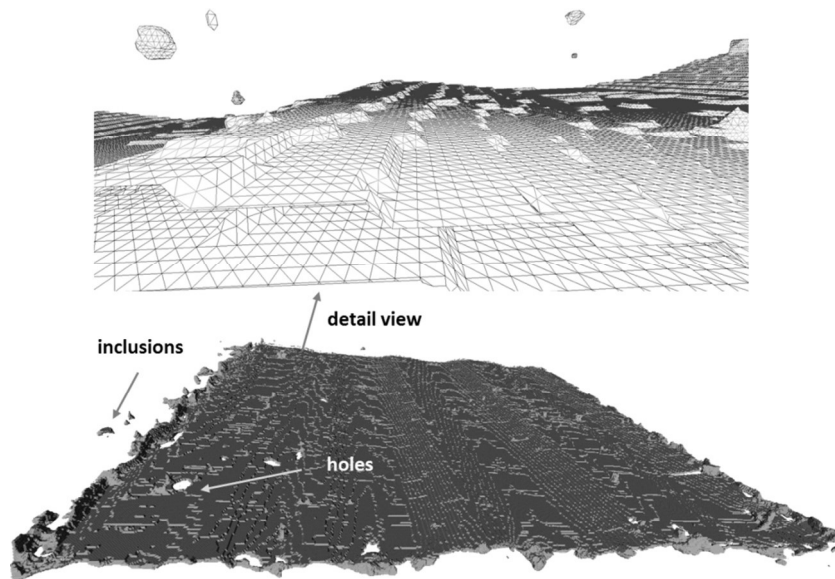**Fig. 7.** Extraction routine for realistic geometries of discontinuities.

Fig. 8. Example of 3D surface mesh of the artificial delamination resultant from the surface extraction tool of "VG Studio Max 2.1".

tribute to the overall geometry, but would cause tremendous increase of computational complexity.

3.2.1.2. Reconstruction. The gray value based threshold extraction method and the removal of the defective surfaces in the previous step may result in holes in the mesh structure. As these are either artificially, or are considered unnecessary details, for closing the holes a reconstruction algorithm is needed. Within "MeshLab" holes can be automatically or manually closed based on a dimensional threshold value, which also prevents the further creation of self-intersecting faces.

3.2.1.3. Simplification. In the present example, the initial mesh network contains 303685 vertices and 610297 faces. This high number of surface elements describes the delamination surface with great accuracy, but may lead to unnecessarily high computational loads. Thus suitable simplification should be considered, which can be done with multiple algorithms in "MeshLab". One approach that was found fairly useful is the "Quadratic Edge Collapse Decimation" which is able to significantly reduce the number of mesh vertices and faces, but still preserves the topology of the surface [63]. After applying this simplification algorithm the mesh network was reduced by 99.5% to 1364 vertices and 3038 faces.

3.2.1.4. Smoothing. At this stage, the mesh structure would be sufficient to be imported in a FEM program for further processing. However, surface smoothing was found to be particularly useful to improve the final quality of the mesh.

This step is applied to facilitate the creation of the volume mesh in the FEM program, which can be highly affected by the presence of distorted elements. For this purpose we used the "Taubin smooth" algorithm, which makes a two-step smoothing, forward and backward, for each iteration [64,65]. The "MeshLab" default values of the smoothing parameters were used with satisfactory results.

The so obtained surface mesh structure is shown in Fig. 9. As additional examples for typical internal discontinuities, extracted volume porosity, a local damage zone in a cross-ply specimen and the damage zone due to impact damage is shown in Fig. 9 as well.

After the post-processing within the "MeshLab" environment, the final geometry is imported in "Comsol Multiphysics" using the "CAD import Module" as mesh sequence in .stl format. Being such a complex surface the import requires a manual face partitioning with the default parameters being changed. The most important parameter is the "maximum boundary neighbor angle" which should have a value close to 0° in order to import all minimally angled faces accurately. The surface to volume transformation is then automatically done within the "Comsol Multiphysics 5.2a" version.

3.2.2. Material properties, applied physics and discretization settings

The properties of the composite sample are reported in Table 2, which were derived from mechanical measurements for 60% fiber volume fraction. As the composite laminate is purely unidirectional, the medium is considered as homogeneous linear elastic anisotropic continuum.

In Fig. 10 all steps followed to implement the geometric boundary constraints in the FEM environment are presented. The composite specimen is a simple plate-like geometry with the imported artificial delamination at the designated depth position and a ROI given by a cylinder with the same diameter as the delay line of the transducer. The main operations to finish the setup are

Table 2
Elastic properties of the composite material.

Property	Sigrafil CE1250-230-39 (unidirectional, 60% FVF)
Density [kg/m^3]	1550
Elastic modulus [GPa]	$C_{11} = 133.42$
	$C_{22} = C_{33} = 12.90$
	$C_{12} = C_{13} = 7.15$
	$C_{44} = 2.06$
	$C_{55} = C_{66} = 6.1$

the Boolean difference to subtract the delamination volume from the specimen plate and a final Boolean intersection to yield only the volume below the transducer.

For the UT modeling, the 2D axisymmetric model of the transducer is coupled to the 3D composite specimen by a displacement mapping between the contact line of the transducer in 2D and the contact surface of the 3D specimen. As graphical representation of this coupling, a 270° revolved view of the transducer is shown located on top of the sample presented in Fig. 10b. The sufficiency of this configuration was validated beforehand against a full 3D model with the transducer in place.

In addition to the settings of the transducer described in 3.1.2 the in-plane surfaces of the ROI are defined as *low reflecting boundary condition*. This is an artificially absorbing layer with matching impedance to let the ultrasonic waves leave the ROI and to avoid unwanted reflections from these surfaces. The mesh element size for the composite plate which were found to lead to a convergent solution are using an [0.1…0.25] mm interval with a maximum element growth rate of 1.3 relative to the neighboring elements. This setting also fulfills the $\lambda/5$ condition as introduced in Section 3.1.2.

A comparison of the modeled A-scan for the reference case (without artificial delamination) and the corresponding experimental A-scan is presented in Fig. 11. The good agreement between the modeled signal and those obtained experimentally validates the used configuration and material properties of the composite laminate. Thus this configuration seems sufficient to perform investigations of the interaction of the ultrasonic wave with the artificial delamination.
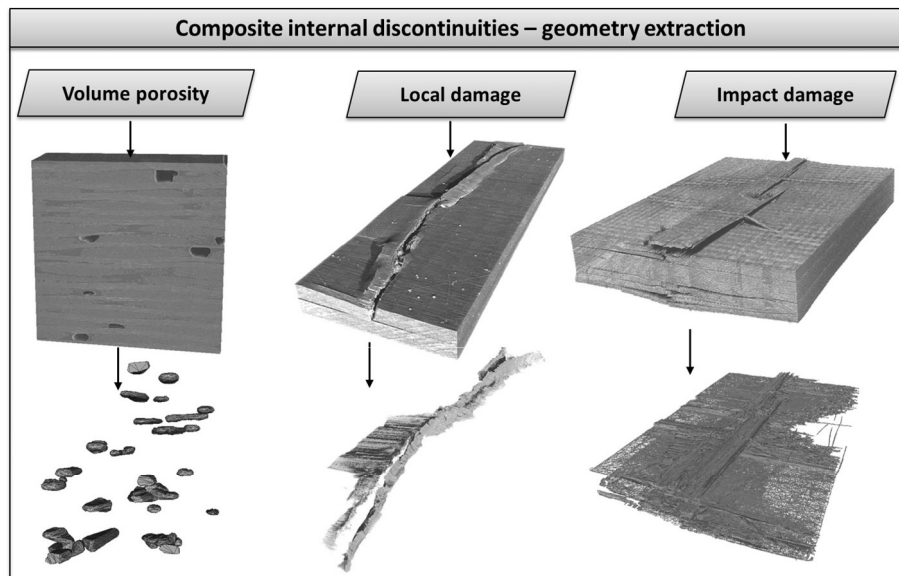

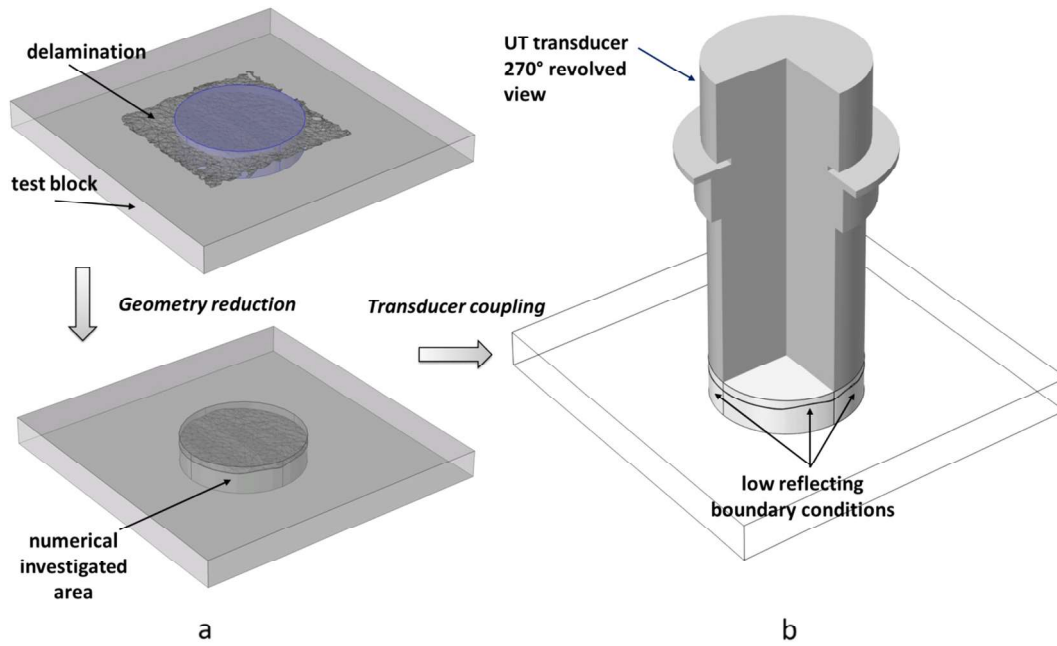**Fig. 9.** Example of typical internal discontinuities extracted geometry.

Fig. 10. Final model geometry of the investigated area (a) and of the sensor with 2D axial symmetry being linked to the 3D sample (b).
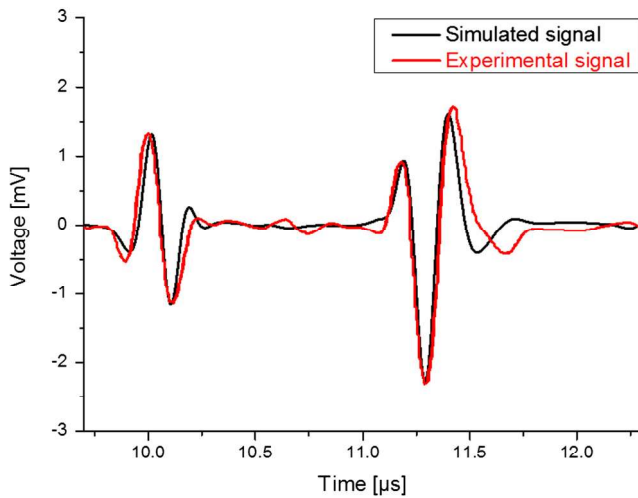

Fig. 11. Typical voltage–thickness simulated vs. measured response for an undamaged composite laminate (reference signal).

4. Results and discussion

In the following, results from numerical modeling are compared to experimental signals as detected from the UT of artificial delamination. The results are presented using the A-scan signals but also using snapshots on slices within the modeled volume showing the structural velocity at distinct time intervals. The first case studied is the one corresponding to the center position (I) of the UT transducer being directly located on top of the delaminated area.

The modeled wave-field for this case is shown in Fig. 12a and b.

The delamination causes 100% reflection of the incident ultrasonic wave, causing no transmission to the lower part of the specimen. The interaction between incident wave field and delamination surface is presented for the same cross section at subsequent time steps. The arrival of the wave field at the delamination occurs at around 5.14 μs.

To assess the influence of the delamination topology, the extracted artificial delamination is compared to a simple flat representation at equivalent depth position (see Fig. 13). In direct comparison, there are obvious differences seen in the wave fields during the first arrival of the wave at the delamination. The surface topology of the CT extracted delamination geometry affects the way in which the incident field is reflected back. This effect of the surface topology is also present in the resulting A-scans seen in Fig. 13. Only the A-scan signal given by the CT extracted geometry fits the experimental data well in terms of amplitude and arrival time. For the perfectly flat delamination geometry, the reflection echo is much higher in amplitude than observed in the experimental A-scan signal.

In Fig. 14, results from the measurement at position (III) at the edge of the delamination and corresponding modeling results are presented. In addition, the sample geometry used for the numerical models is shown. Fig. 14a shows the A-scan of the CT-extracted delamination model compared with the experimental A-scan. A good agreement is observed for these two signals in terms of surface echo amplitude, delamination echo amplitude and back wall echo amplitude. For the second implementation the delamination geometry is chosen perfectly flat at equivalent depth position to the CT extracted case. For this approach, major differences are seen when comparing the amplitude of the delamination echo. In the flat delamination case the reflected wave amplitude is significantly higher than in the model with the CT extracted geometry. Even a second delamination echo is detected within the 10.6 μs before the arrival of the backwall echo (cf. Fig. 14b).

5. Conclusions

Quantitative modeling of ultrasonic inspection using FEM tools is able to provide very good description of ultrasonic wave interaction with defects when realistic geometries of the internal discontinuities are taken into account. The validity of the approach was presented by implementation of a realistic transducer model and by considering the anisotropic nature of the propagation medium.
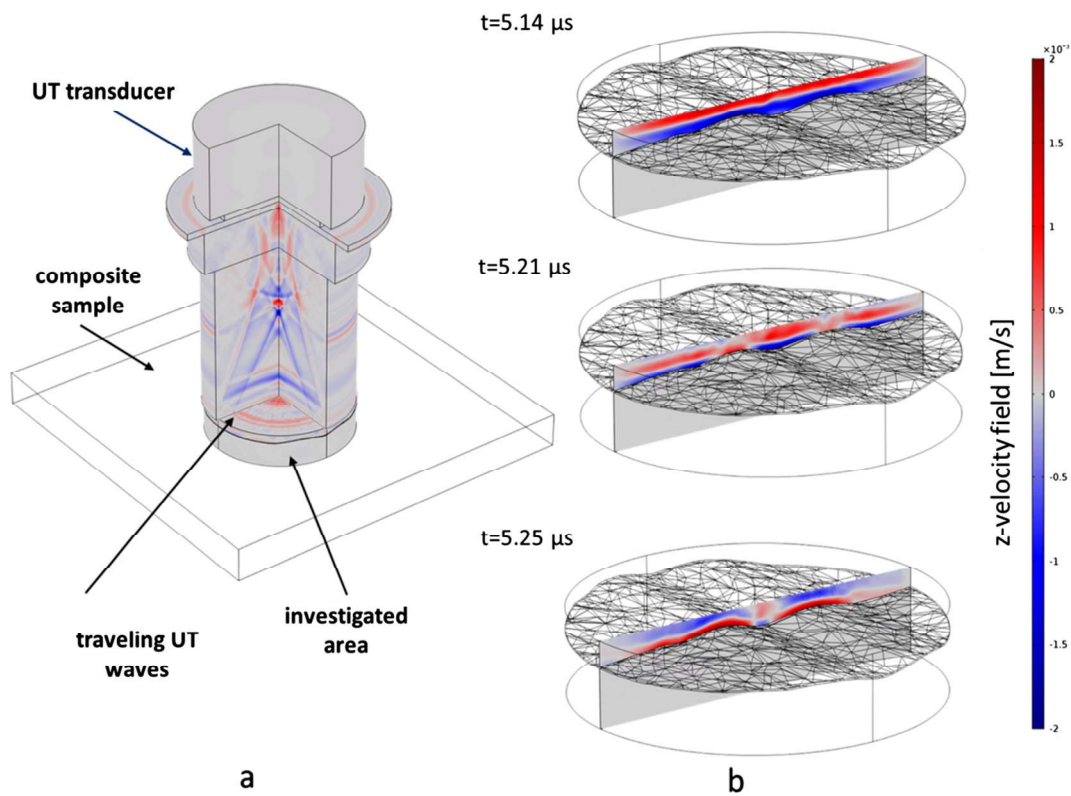
Fig. 12. Calculated UT waves propagating in the 270° revolved transducer (a) and in sample volume with delamination (b).
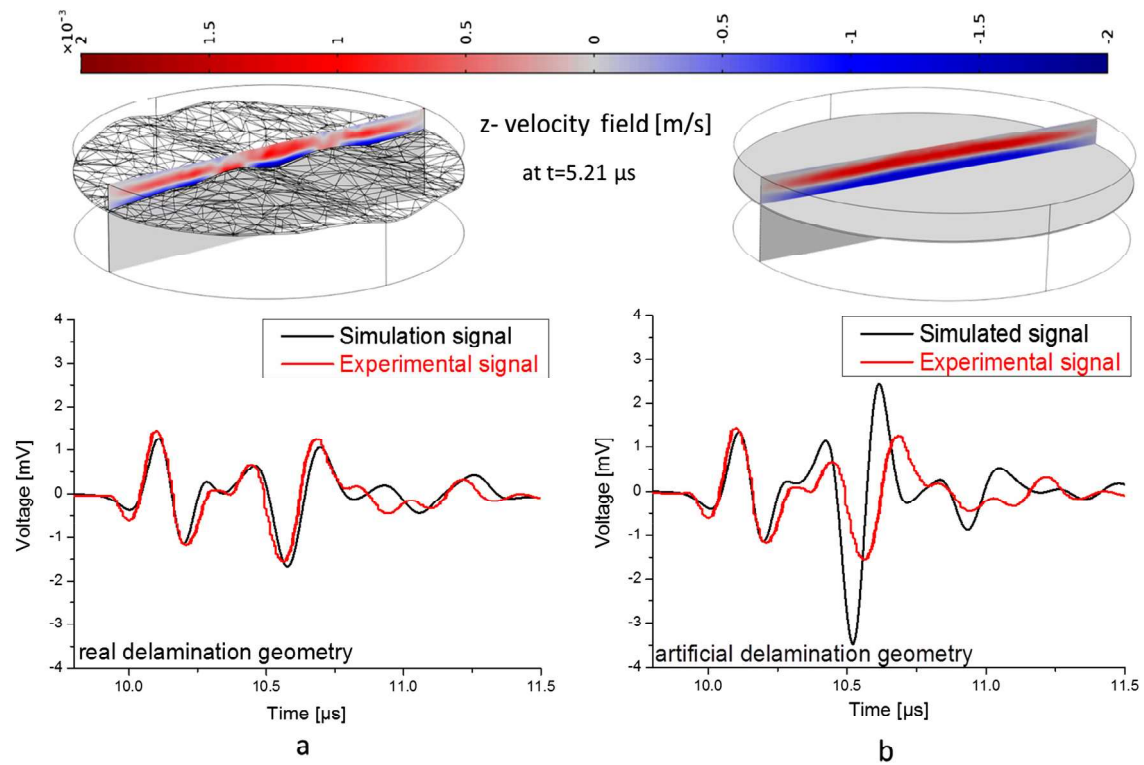

Fig. 13. Calculated UT waves for the center case transducer location with CT-extracted delamination (a) and perfectly flat delamination (b).

To extract realistic geometries for internal discontinuities, a procedure was proposed to obtain surface meshes from volumetric data, which can be refined to be embedded in numerical tools.

The comparison of the modeled A-scan signals with experimental A-scan signals provides very good agreement for the example using the geometry implementation of an artificial delamination
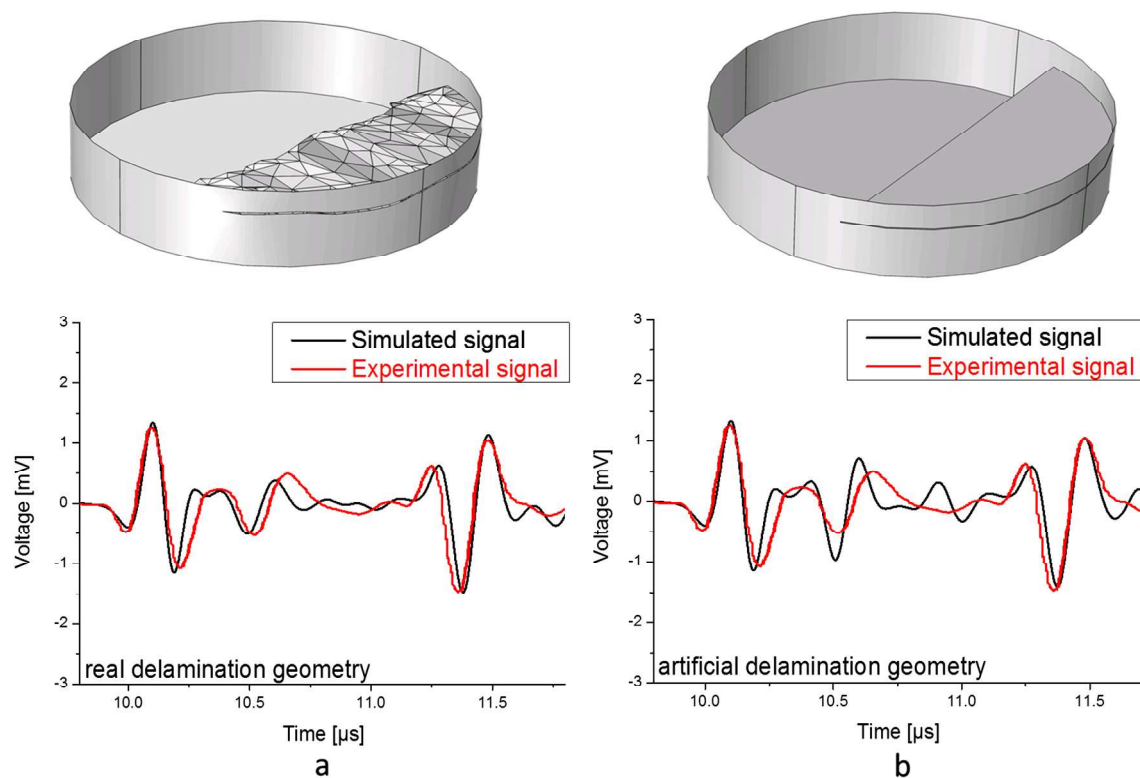
Fig. 14. Comparison of experimental and modeled A-scan signals for the transducer position at the edge of the delamination with CT extracted delamination (a) and perfectly flat delamination (b).

based on CT data. Similar, the discrepancy for modeled A-scans using more simple geometric representations to the experimental A-scans underlines the importance of this approach.

The proposed method for reconstructing the internal geometry of typical discontinuities is not only limited to the case of artificial delamination demonstrated herein, but is even more suitable for complex damage zones such as occurring after impact damage. Likewise, similar approaches might prove interesting to also represent the internal textile structure of fiber reinforced composites, such as fiber bundles, rovings, tapes and similar meso-structures.

Acknowledgments

References

[1] S. Journiac, N. Leymarie, N. Dominguez, C. Potel, Simulation of ultrasonic inspection of composite using bulk waves: application to curved components, J. Phys: Conf. Ser. 269 (2011).

[2] V. Giurgiutiu, G. Santoni-Bottai, Structural health monitoring of composite structures with piezoelectric-wafer, Active Sensors 49 (3) (2011) 565–581.

[3] M.G.R. Sause, S. Horn, Simulation of acoustic emission in planar carbon fiber reinforced plastic specimens, J. Nondestruct. Eval. 2010 (29) (2010) 123–142.

[4] S. Giannis, K. Hansen, R.H. Martin, Accounting for the R-curve Effects on the Mode I Fatigue Delamination Growth Characterization of Unidirectional Composites, in: Proceedings of the American Society for Composites Twenty-fifth Technical Conference, 2010.

[5] G.B. Murri, Effect of data reduction and fiber-bridging on Mode I delamination characterization of unidirectional composites, J. Compos. Mater. 48 (19) (2014) 2413–2424.

[6] P. Cawley, The rapid non-destructive inspection of large composite structures, Composites 25 (5) (1994) 351–357, http://dx.doi.org/10.1016/S0010-4361(94)80005-7.

[7] M. G. R. Sause, R. Stößel, R. Oster, R. Söhnchen, P. Jahnke, A. Seemann, M. Goldammer, C.U. Grosse, "MAIzfp – A Joint Research Effort on NDT of Fiber Reinforced Composites within the Leading-Edge Cluster MAI Carbon, in: Proc. 19th World Conference on Non-Destructive Testing, Munich, 2016.

[8] S. Gholizadeh, A review of non-destructive testing methods of composite materials, Procedia Struct. Integrity 1 (2016) 50–57, http://dx.doi.org/10.1016/j.prostr.2016.02.008.

[9] S. Grondel, J. Assaad, C. Delebarre, E. Moulin, Health monitoring of a composite wingbox structure, Ultrasonics 42 (2004) 819–824.

[10] N.G.H., Meyendorf, P.B. Nagy,S. Rokhlin, Nondestructive Materials Characterization: With Applications to Aerospace Materials, Springer, 2013.

[11] C. Meola, G.M. Carlomagno, Infrared thermography to evaluate impact damage in glass/epoxy with manufacturing defects, Int. J. Impact Eng 67 (2014) 1–11, http://dx.doi.org/10.1016/j.ijimpeng.2013.12.010.

[12] M. Spies, Analytical methods for modeling of ultrasonic nondestructive testing of anisotropic media, Ultrasonics 42 (1-9) (2004) 213–219.

[13] A.F. Grandt, Fundamentals of Structural Integrity, John Wiley & Sons, Inc., 2004 (Section 1.5).

[14] J. Brown, POD test – it takes more than a statistician to do probability of detection, Mater. Eval. 4 (2012) 421–426.

[15] J.H. Kurz, A. Jüngert, S. Dugan, G. Dobmann, Probability of Detection (POD) determination using ultrasound phased array for considering NDT in probabilistic damage assessments, World Conference on Nondestructive Testing, paper 329, 2012.

[16] C. Annis, Nondestructive Evaluation System Reliability Assessment, Wright-Patterson AFB USA, 2009.

[17] A.P. Berens, NDE Reliability Data Analysis, Nondestructive Evaluation and Quality Control 3rd ed., vol.17, 1994, pp. 689–701.

[18] N. Dominguez, F. Jenson, Simulation Assisted POD of a High Frequency Eddy Current Inspection Procedure, in: 10th European Conference on Non-Destructive Testing, 2010.

[19] C.R.A. Schneider, R.M. Sanderson, C. Carpentier, L. Zhao, C. Nageswaran, Estimation of probability of detection curves based on theoretical simulation of the inspection process, BINDT Annual Conference, 2012.

[20] F. Jenson, S. Mahaut, P.Calmon, et al., Simulation based POD evaluation of NDI techniques, in: 10th European Conference on Non-Destructive Testing, 2010.

[21] F. Schubert, H. Baron, J. Menges, V. Dorval, C. Gilles-Pascaud, R. Raillon-picot, N. Dominguez, J. Chatellier, T. Barden, Simulation-Supported POD for Ultrasonic Testing – Recommendations from the PICASSO Project, e-J. Nondestruct. Test., vol.19, no. 5, 2013.

[22] M. Carboni, S.A. Cantini, Model Assisted Probability of Detection approach for ultrasonic inspection of railway axles, in: 18th World Conference on Non-Destructive Testing, 2012.

[23] Model Assisted POD working group. http://www.cnde.iastate.edu/MAPOD (accessed in 21.11.2016).

[24] S. Deydier, N. Leymarie, P. Calmon,V. Mengeling, Modeling of the ultrasonic propagation into carbon-fiber-reinforced epoxy composites, using a ray theory based homogenization method, AIP Conf. Proc., vol. 820, no. 972, 2006. 10.1063/1.2184630.

[25] Z. You, M. Lusk, R. Ludwig, W. Lord, Numerical simulation of ultrasonic wave propagation in anisotropic and attenuative solid materials, IEEE Transact. Ultrason., Ferroelect. Freq. Control 38 (5) (1991) 436–445.

[26] R. Ludwig, W. Lord, A finite-element formulation for the study of ultrasonic NDT systems, IEEE Transact. Ultrason., Ferroel. Freq. Control 35 (6) (1988) 809–819.

[27] W. Lord, R. Ludwig, Z. You, Developments in ultrasonic modeling with finite element analysis, J. Nondestruct. Eval. 9 (129) (1990), http://dx.doi.org/10.1007/BF00566389.

[28] J.A.G. Temple, Modeling the propagation and scattering of elastic waves in inhomogeneous anisotropica media, J. Phys. D 21 (1988) 859–874.

[29] R. Ludwig, The Finite Element Modeling of Ultrasonic NDT Phenomena, Ph.D. dissertation, Colorado State University, 1986.

[30] R.A. Roberts, Computational prediction of micro-crack induced ultrasound attenuation in CFRP composites, J. Nondestruct. Eval. 33 (443) (2014), http://dx.doi.org/10.1007/s10921-014-0240-1.

[31] H.J. Kim, S.J. Song, L.W. Schmerr, Modeling ultrasonic pulse-echo signals from a flat-bottom hole in immersion testing using a multi-gaussian beam, J. Nondestruct. Eval. 23 (11) (2004), http://dx.doi.org/10.1023/B:JONE.0000045217.48147.f6.

[32] M. Rudolph, Ultrasonic Beam Models in Anisotropic Media, Ph.D. Dissertation, Iowa State University, 1999.

[33] P. Calmon, Trends and Stakes of NDT Simulation, J. Nondestruct. Eval. 31 (339) (2012), http://dx.doi.org/10.1007/s10921-012-0152-x.

[34] PICASSO project. http://www.picasso-ndt.eu/ (accessed in 15.12.2016).

[35] S. Mahaut et al. Simulation of complex ultrasonic NDT cases using coupled analytical-numerical method: the Mohycan project, in: Proc. of the 10th European Conference of NDT, 2010.

[36] K. Kapoor, K.S. Krishna, S.A. Bakshu, On parameters affecting the sensitivity of ultrasonic testing of tubes: experimental and simulation, J. Nondestruct. Eval. 35 (56) (2016), http://dx.doi.org/10.1007/s10921-016-0371-7.

[37] CIVA software platform for simulating NDT techniques (UT, EC, RT) http://www-civa.cea.fr (accessed in 16.11.2016).

[38] T. Kundu, D. Placko, E.K. Rahani, T. Yanagita, C.M. Dao, Ultrasonic field modeling: a comparison between analytical, semi-analytical and numerical techniques, IEEE Transact. Ultrason., Ferroelect. Freq. Control 57 (12) (2010) 2795–2807, http://dx.doi.org/10.1109/TUFFC.2010.1753.

[39] T. Kundu, Ultrasonic and electromagnetic waves for nondestructive evaluation and structural health monitoring, Structural Integrity Elsevier Ltd 86 (2012) 395–405, http://dx.doi.org/10.1016/j.proeng.2014.11.053.

[40] M. Darmon, N. Leymarie, S. Chatillon, S. Mahaut, Ultrasonic Wave Propagation in Non Homogeneous Media, Springer, 2009, pp. 70.

[41] P.G. Young, T.B.H. Beresford-West, S.R.L. Coward, B. Notarberardino, B. Walker, A. Abdul-Aziz, An efficient approach to converting three-dimensional image data into highly accurate computational models, Phil. Trans. Roy. Soc. A 366 (2008) 3155–3173, http://dx.doi.org/10.1098/rsta.2008.0090.

[42] V.M. Arbour, E. Snively, Finite element analyses of ankylosaurid dinosaur tail club impacts, Anat. Rec. 292 (9) (2009) 1412–1426, http://dx.doi.org/10.1002/ar.

[43] C.A. Mota Soares, C.M. Mota Soares, M.J.M. Freitas, Mechanics of Composite Materials and Structures, NATO Science Series, vol. 361, 1999.

[44] C. Hanxin, S. Zhang, R. King, M.G. Pecht, Simulation of ultrasonic testing technique by finite element method, in: Proceedings of the IEEE Prognostics and System Health Management Conference, 2012, 10.1109/PHM.2012.6228959.

[45] G. Baskaran, C.L. Rao, K. Balasubramaniam, Simulation of the TOFD technique using the finite element method, INSIGHT 49 (11) (2007) 641–646.

[46] J. Sun, H. Zhao, X. Han, et al., Ultrasonic test of groove base on finite element method, J. Metrol. Measur. Technol. 6 (9) (2009).

[47] W. Dong, Z. Zhenggan, Finite difference simulation of pulsed ultrasonic propagation in solids, J. Acta Aeronautica et Astronautica Sinica 31 (2) (2010) 388–392.

[48] O. Cervena, P. Hora, Analysis of the conical piezoelectric acoustic emission transducer, Appl. Comput. Mech. 2 (2008) 13–24.

[49] A-M Zelenyak, R. Oster, M. Mosch, P. Jahnke, M.G.R. Sause, Numerical Modeling of Ultrasonic Inspection in Fiber Reinforced Materials with Explicit Microstructure, in: 19th World Conference on NDT, München, 2016.

[50] J. Prikšaitis, L. Mažeika, R. Barauskas, E. Žukauskas, A. Kriščiūnas, Influence of the numerical dispersion effects in the modelling of ultrasonic measurements, Phys. Proced. 70 (2015) 532–536, http://dx.doi.org/10.1016/j.phpro.2015.08.010.

[51] A. Bacigalupo, L. Gambarotta, Second-order computational homogenization of heterogeneous materials with periodic microstructure, ZAMM Z. Angew. Math. Mech. 90 (10–11) (2010) 796–811.

[52] V.G. Kouznetsova, M.G.D. Geers, W.A.M. Brekelmans, Multi-scale second-order computational homogenization of multi-phase materials:a nested finite element solution strategy, Comput. Methods Appl. Mech. Eng. 193 (2004) 5525–5550.

[53] K.W. Pratt, Digital image Processing, 3rd ed., Willey, 2001, pp. 551–587.

[54] N. Memom, A. Mirza, S.A.M. Gilani, Deficiencies of lung segmentation techniques using CT scan images for CAD, World Acad. Sci., Eng. Technol. 20 (2006) 108–112.

[55] N. Mesanovic, M.Grgic, H. Huseinagic, et al. Automatic CT image segmentation of the lungs with region growing algorithm, in: 18th International Conference on Systems,Signals and ImageProcessing, 2011, pp. 395–400.

[56] B. Van Ginneken, A.F. Frangi, J.J. Staal, et al., "Active shape model segmentation with optimal features, J. Med. Imaging IEEE Transact. 21 (8) (2002) 924–933, http://dx.doi.org/10.1109/TMI.2002.80312.

[57] M. Kass, A. Witkin, D. Terzopoulos, Snakes: Active contourmodels, Int. J. Comput. Vis. 1 (4) (1988) 321–331.

[58] T. McInerney, D. Terzopoulos, Deformable models in medical image analysis: a survey, Med. Image Anal. 1 (2) (1996) 91–108.

[59] J.A. Sethian, Level Set Methods and Fast Marching Methods, 2 ed., Cambridge Univ. Press, Cambridge, U.K., 1999.

[60] J.A. Sethian, Level Set Methods and Fast Marching Methods, 2nd ed., Cambridge Univ. Press, Cambridge, U.K., 1999.

[61] T.F. Cootes, C.J. Taylor, D. Cooper, J. Graham, Active shape models—Their training and applications, Comput. Vis. Image Understanding 6 (1) (1995) 38–59.

[62] G. Behiels, D. Vandermeulen, F. Maes, P. Suetens, P. Dewaele, Active shape model-based segmentation of digital X-ray images, MICCAI 99 (1999) 128–137.

[63] H. Hoppe, New Quadric Metric for Simplifying Meshes with Appearance Attributes, Proceedings VIS, 1999.

[64] G. Taubin, Curve and surface smoothing without shrinkage, Technical Report RC-19536 IBM Research, 1994.

[65] G.Taubin, A signal processing approach to fair surface design, Proceedings of SIGGRAPH, 1995, pp. 351–358.